ARTICLE

Solvent selection as a major determinant of chiral resolution outcomes: The BINOL-DACH case study

Received 00th January 20xx,
Accepted 00th January 20xx

DOI: 10.1039/x0xx00000x

Joséphine de Meester[a, b], Oleksii Shemchuk[a], Laurent Collard[a], Johan Wouters[b], Koen Robeyns[a], Tom Leyssens[a]

In this study, we undertook an in-depth study of the combination of two chiral molecules: 1,1'-Bi-2-naphtol (BINOL) and *trans*-Cyclohexane-1,2-diamine (DACH). While exploring various solvents for developing resolution processes, we revealed a multitude of solid phases. Here is analyzed the different crystalline forms obtained in the selected solvents, underscoring the critical importance of the solvent choice for the development of a chiral resolution process.

Introduction

Chirality plays a pivotal role, influencing a spectrum of chemical and biological processes across various fields, including pharmaceuticals, material science, catalysis, and agronomy.[1,2] The separation of enantiomers, non-superimposable mirror images, is of fundamental importance for these fields and can be achieved through various methods.[2–5] Processes based on crystallization are among the most widespread, due to their advantages in terms of economical consumption and ease of industrialization.[1–3,6] Over the recent years, cocrystallization has shown some unexplored potential in the context of chiral resolution, leading to the development of enantiospecific[7,8] and diastereomeric[9,10] cocrystal resolution processes, the establishment of chiral matrices with selective inclusion cavities targeting a specific enantiomer,[2,3,9] and the transformation of racemic compounds into conglomerates which can ultimately be used in the context of preferential crystallization.[11–14]

When investigating resolution potential, researchers often mainly focus on the solid-state nature of the parent compounds, introducing solvent selection at a later stage. However, in a recent contribution, we underscored the critical role of solvent selection in resolution processes, demonstrating how a mere switch of the solvent nature drastically altered the direction of resolution.[15]

In this study, we further highlight the importance of the achiral solvent in the context of resolution, focusing on BINOL, and combining it with *trans*-cyclohexane-1,2-diamine (DACH) (Figure 1). Two diastereomeric cocrystals of this system – (*R*)-BINOL-(*R,R*)-DACH (*R-RR*) and (*S*)-BINOL-(*R,R*)-DACH (*S-RR*) – are already reported in literature along with a (*R*)-BINOL-(*R,R*)-DACH-toluene (*R-RR*-tolu) cocrystal-solvate.[16] Intuitively this system would qualify for diastereomeric resolution. However, we underline here the importance of solvent selection for such a process, highlighting the solid form landscape of BINOL-DACH chiral combinations in various solvent environments. The participation of the solvent to the solid forms (solvatism) is of crucial importance for the outcome of the crystallization, and thus also for the resolution potential of the system.

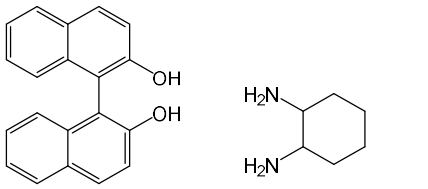

1,1'-bi-2-naphthol *trans*-cyclohexane-1,2-diamine

Figure 1. Molecular structures of BINOL and DACH.

Materials and methods

Materials

(*S*)-1,1'-Bi-2-naphtol (Merck), (*R*)-1,1'-Bi-2-naphtol (Fluorochem), (*rac*)-1,1'-Bi-2-naphtol (Acros Organics), (*1S,2S*)-*trans*-Cyclohexane-1,2-diamine (Apollo Scientific), (*1R,2R*)-*trans*-Cyclohexane-1,2-diamine (Apollo Scientific), (*rac*)-*trans*-Cyclohexane-1,2-diamine (Thermo scientific), toluene (VWR chemicals), benzene (TCI), methanol (VWR chemicals), acetonitrile (VWR chemicals), ethanol (VWR chemicals), and ethyl acetate (VWR chemicals) were

[a] Institute of Condensed Matter and Nanosciences, UCLouvain, Place Louis Pasteur 1, 1348 Louvain-la-Neuve, Belgium E-mail: tom.leyssens@uclouvain.be
[b] Department of Chemistry, Université de Namur, UNamur, Rue de Bruxelles 61, 5000 Namur, Belgium
Supplementary Information available. See DOI: 10.1039/x0xx00000x

purchased from commercial sources and used without further purification.

Slurry experiments

Slurry experiments were performed preparing equimolar suspensions (1 mmol) of BINOL with DACH at 20°C in toluene, benzene, methanol, acetonitrile, ethanol, and ethyl acetate (V=1-1.5 mL). The suspensions were stirred in a Cooling thermomixer HLC at 500 rpm. After 1 day of stirring, all vials were seeded with all possible crystalline forms and then left to equilibrate for 7 days. The suspensions were filtered, the powders were washed, dried and analyzed using XRPD, while the remaining solutions were not systematically analyzed.

Single Crystal Formation

1) By cooling

Single crystals of (*rac*)-BINOL-(*rac*)-DACH-EtOAc (*rac-rac*-EtOAc) and (*rac*)-BINOL-(*rac*)-DACH-MeOH (*rac-rac*-MeOH) were obtained by cooling crystallization from the solvent, starting from an undersaturated equimolar solution of BINOL and DACH at RT. The vials were placed at 9°C. Once crystals formed, a suitable crystal was retrieved and analyzed by SC-XRD. As one crystal does not necessarily represent the entire bulk material, homogeneity was checked by comparing the simulated XRPD patterns from single-crystal structures with the experimental XRPD patterns of the slurries.

2) By slow evaporation

Single crystals of (*R*)-BINOL-(*R,R*)-DACH-benzene (*R-RR*-benz), (*rac*)-BINOL-(*rac*)-DACH (*rac-rac*), and (*rac*)-BINOL-(*R,R*)-DACH-EtOH (*rac-RR*-EtOH) were obtained by slow evaporative crystallization from the different solvents, starting from an undersaturated equimolar solution of BINOL and DACH. The solution was left to evaporate slowly at RT. Once crystals formed, a suitable crystal was retrieved and analyzed by SC-XRD. As one crystal does not necessarily represent the entire bulk material, homogeneity was checked by comparing the simulated XRPD patterns from single-crystal structures with the experimental XRPD patterns of the slurries.

Thermal analyses

1) Thermogravimetric analyses (TGA)

TGA analyses were conducted using a Mettler Toledo TGA/DSC 3+ instrument, varying the temperature from 25 to 600°C, with a heating rate of 10°C/min, under nitrogen with a flow rate of 50mL/min. Solid samples (5-10 mg) were placed in alumina pans.

2) Differential scanning calorimetry analyses (DSC)

DSC analyses were conducted using a TA Instrument DSC2500. The temperature range employed for the analyses was from 25°C to *desired temperature* (determined through TGA), at a heating rate of 5°C/min under nitrogen with a flow rate of 50 mL/min. Solid samples (5-10 mg) were placed in aluminum pans with perforated lid.

X-ray powder diffraction (XRPD)

XRPD data were collected using either a Siemens D5000 diffractometer or a Bruker D8 Discover diffractometer. Both are equipped with a Cu X-ray source operating at 40 kV and 40 mA. A secondary monochromator was used to select the Kα radiation of Cu (λ = 1.5418 Å). A scanning range of 2θ values was applied from 5° to 35° or 5° to 25°.

Single crystal X-ray diffraction (SC-XRD)

SC-XRD data were collected on a MAR345 image plate detector using Mo Kα radiation (λ = 0.71073 Å), generated by an Incoatec IμS microfocus source. All datasets were measured at ambient conditions, except for the redetermination of the *R-RR* cocrystal (CDCC ref code: DIFFOO[16]), which was performed at 150K. The collected data was integrated and reduced using CrysAlis^{PRO} [17] and the implemented absorption correction was applied. Structure solution was achieved using the dual-space algorithm in SHELXT[18] and the structure was further refined against F^2 by SHELXL.[19] Non-hydrogen atoms were refined anisotropically and all CH atoms were added in calculated positions. The hydrogens involved in hydrogen bonds could be located in the density maps. For the structures *R-RR*-benz, *rac-rac*-EtOAc, and *rac-rac* the COH angle is idealized and the hydrogen was allowed to rotate and the OH distanced allowed to vary, NH hydrogens were allowed to refine freely. For 4*rac*-4*RR*-3EtOH.H_2O the OH and NH hydrogens could be located in the density maps but were refined with restrained/idealized N/O-H distances and C-N/O-H angles, OH hydrogens on the solvent molecules were refined with idealized O-H distances and X-O-H angles. For *rac-rac*-MeOH the hydrogen bonded H atoms were also found in the density maps, the OH hydrogens were set at an idealized angle, the O-H distances were allowed to vary; as the NH groups were disordered, bond and angle restraints were used for the NH_2 groups and the NH_3 groups were idealized but allowed to rotate. Symmetry analysis and validation were carried out using PLATON.[20] Figures were generated using the molecular visualization software Mercury v4.3.4.[21]

CCDC 2470279-2470284 contain the supplementary crystallographic data for this paper. These data can be obtained free of charge from The Cambridge Crystallographic Data Centre via www.ccdc.cam.ac.uk/structures.

Chiral High-Performance Liquid Chromatography (cHPLC)

The separation of (*R*)- and (*S*)-BINOL was performed by Chiral HPLC using a Waters Arc HPLC coupled with a 2998 PDA detector. Both enantiomers of BINOL were separated on a Daicel Chiralpak IA column 250 x 4.6 mm 5 µm with a mix of 90 vol.% isohexane, 10 vol.% isopropanol as mobile phase. The separation was performed at 25°C with a flow rate of 1 mL/min.[15]

Nuclear magnetic resonance (NMR)

^{1}H NMR spectra were measured either on a 300 MHz or on a 400 MHz spectrometer (Bruker). Chemical shifts are reported in parts per million (ppm) and were referenced regarding the chemical shift of the peak of the deuterated solvent used ($(CD_3)_2SO$ at 2.50 ppm).

Spectral multiplicities are described as follows: singlet (s), doublet (d), triplet (t), quartet (q), and multiplet (m).^{1}H NMR of BINOL (300 MHz, DMSO) δ 9.21 (s, 2H), 7.92 – 7.78 (m, 4H), 7.31 (d, *J* = 8.9 Hz, 2H), 7.26 – 7.11 (m, *J* = 20.0, 8.1, 6.8, 1.3 Hz, 4H), 6.93 (d, *J* = 8.1 Hz, 2H).
^{1}H NMR of DACH (300 MHz, DMSO) δ 2.09 – 1.96 (m, 2H), 1.75 – 1.65 (m, 2H), 1.61 – 1.53 (m, 2H), 1.21 – 1.10 (m, 2H), 1.02 – 0.89 (m, 2H).

Results and discussion

To explore the possible outcomes when combining BINOL and DACH (Figure 1), varying their stereochemistry, five combinations need to be considered (Table 1). All other combinations can be obtained by mirror symmetry. As the *R-RR* and *S-RR* cocrystals, and the *R-RR*-toluene cocrystal-solvate have already been described in the literature[16] and a complex *R-RR*-benzene suspected to form,[22] we decided to focus on investigating the impact of solvatism on the outcome of the five combinations shown in Table 1 concentrating on six different solvents (Table 2). Besides toluene and benzene (chosen to compare our results with those reported in the literature), four other solvents were selected with different polarity and proticity. The chosen solvents can be divided into three groups: non-polar and aprotic solvents toluene and benzene; polar and aprotic solvents ethyl acetate (EtOAc) and acetonitrile (ACN); and polar and protic solvents methanol (MeOH) and ethanol (EtOH).

All solvent-based experiments were performed using an equimolar mixture of BINOL:DACH (1:1) as this is also the stoichiometry of the already reported cocrystals.

Table 1. The five studied combinations between BINOL and DACH.

Stereochemical combination			Mirror image symmetry		
(*R*)-BINOL	+	(*R,R*)-DACH	(*S*)-BINOL	+	(*S,S*)-DACH
(*S*)-BINOL	+	(*R,R*)-DACH	(*R*)-BINOL	+	(*S,S*)-DACH
(*rac*)-BINOL	+	(*R,R*)-DACH	(*rac*)-BINOL	+	(*S,S*)-DACH
(*R*)-BINOL	+	(*rac*)-DACH	(*S*)-BINOL	+	(*rac*)-DACH
(*rac*)-BINOL	+	(*rac*)-DACH			

A screening process was carried out using three different approaches: by slurrying, cooling, and slow-evaporation. Remarkably, the 30 potential combinations led to the isolation of a total of eleven different crystalline phases. For most combinations, a single solid phase was obtained irrespective of the method used. However, an exception was observed when combining (*rac*)-BINOL and (*rac*)-DACH in EtOAc, for which the slow evaporation and slurry methodologies led to two different crystalline phases.
Out of the eleven phases, eight are herein reported for the first time, five of which structurally characterized: *R-RR*-benz*, rac-rac*, *rac-rac*-EtOAc, *rac-rac*-MeOH, and 4*rac*-4*RR*-3EtOH-1H_2O (Table 2). Crystallographic details of these five phases are reported in Tables 3 and SI-1. It is important to note that, given their very close pK_a[23,24], both salt or cocrystal could be obtained between the two species. Thus, their nature will be determined, when possible, via SC-XRD analysis.

Table 2. Slurry and SC-XRD results of the screening of the five combinations between BINOL and DACH obtained in six different solvents. In blue are colored the multicomponent crystal phases already discovered in the literature[16].

Combination	Toluene	Benzene	EtOAc	ACN	MeOH	EtOH
(*R*)-Binol + (*R,R*)-DACH	*R-RR*-tolu (1:1:1)	*R-RR*-benz[a] (1:1:1)	*R-RR* (1:1)	*R-RR* (1:1)	*R-RR*[a] (1:1)	*R-RR* (1:1)
(*S*)-Binol + (*R,R*)-DACH	*S-RR* (1:1)	*S-RR* (1:1)	*S-RR* (1:1)	*S-RR* (1:1)	*S-RR* (1:1)	*S-RR* (1:1)
(*rac*)-Binol + (*R,R*)-DACH	*R-RR*-tolu (1:1:1)	*R-RR*-benz (1:1:1)	2*rac*-2*RR*-EtOAc[b] (2:2:1)	*R-RR* (1:1)	*rac-RR*-MeOH (1:1:1)	4*rac*-4*RR*-3EtOH-H_2O[a] (4:4:3:1)
(*R*)-Binol + (*rac*)-DACH	*R-RR*-tolu (1:1:1)	*R-RR*-benz (1:1:1)	*R-RR* + *R-SS* (1:1)	*R-RR* (1:1)	*R-RR* (1:1)	*R-RR* (1:1)
(*rac*)-Binol + (*rac*)-DACH	*R-RR*-tolu + *S-SS*-tolu (1:1:1)	*R-RR*-benz + S-SS-benz (1:1:1)	*rac-rac*-EtOAc[a,c] (1:1:1) *rac-rac*[b, d] (1:1)	*rac-rac*[a] (1:1)	*rac-rac*-MeOH[a] (1:1:1)	*rac-rac*-EtOH[b] (1:1:1)

[a] structurally characterized by single crystal X-ray diffraction
[b] not structurally characterized
[c] obtained by slow and evaporation experiment
[d] obtained by a slurry experiment

Table 3. Main crystallographic data for *R-RR*, *R-RR*-benz, 4*rac*-4*RR*-3EtOH-H_2O, *rac-rac*-EtOAc, *rac-rac* and *rac-rac*-MeOH phases.

Crystalline phase	*R-RR*	*R-RR*-benz	4*rac*-4*RR*-3EtOH-H_2O	*rac-rac*-EtOAc	*rac-rac*	*rac-rac*-MeOH
Empirical formula	$C_{26}H_{28}N_2O_2$	$C_{32}H_{34}N_2O_2$	$C_{110}H_{132}N_8O_{12}$	$C_{28}H_{32}N_2O_3$	$C_{26}H_{28}N_2O_2$	$C_{27}H_{32}N_2O_3$
Formula weight [g/mol]	400.50	478.61	1758.23	444.55	400.50	432.54
Temperature [K]	150(2)	297(2)	297(2)	297(2)	297(2)	297(2)
Crystal system	orthorhombic	orthorhombic	triclinic	triclinic	monoclinic	triclinic

Space group	$P2_12_12_1$	$C222_1$	$P1$	$P\text{-}1$	$P2_1/c$	$P\text{-}1$
a [Å]	9.85511(18)	12.3993(15)	10.3936(12)	8.1693(10)	8.1707(5)	10.2697(12)
b [Å]	15.3092(3)	14.0194(10)	11.2508(9)	9.2052(9)	29.731(2)	11.140(2)
c [Å]	28.2920(6)	15.3719(12)	20.951(2)	16.684(2)	9.0449(6)	11.3987(17)
α [°]	90	90	87.176(7)	96.026(9)	90	108.518(16)
β [°]	90	90	89.274(8)	95.209(10)	101.667(6)	101.580(12)
γ [°]	90	90	76.533(8)	102.224(9)	90	101.228(14)
Volume [Å^3]	4268.53(15)	2672.1(4)	2379.6(4)	1211.1(2)	2151.8(3)	1163.6(3)
Z	8	4	1	2	4	2
Flack parameter	0.3(4)	-0.8(10)	0.2(7)			

[a] absolute configurations were assigned based on the known chirality of the starting enantiopure compounds, rather than the Flack parameter values.

Combination 1: (R)-BINOL and (R,R)-DACH

The already reported *R-RR* cocrystal (CDCC ref code: DIFFOO[16]) is obtained when combining (*R*)-BINOL and (*R,R*)-DACH by slurry experiments in EtOAc, ACN, MeOH, and EtOH (Figure SI-1), and its structure was redetermined at 150 K (Table SI-1). The solid is characterized by two formula units in the asymmetric unit (Z'=2). Both pairs have different orientations of the OH and NH_2 hydrogens, resulting in different hydrogen bonding interactions (Figure 2b, Table SI-2), with 1D hydrogen bond chains orthogonal to each other (Figure 2a).

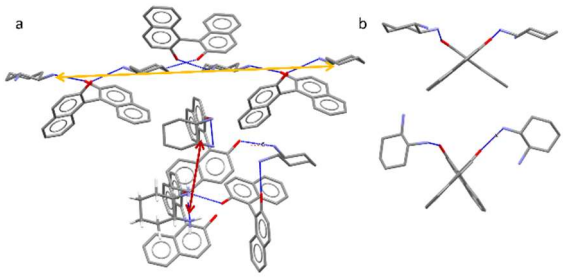

Figure 2. Extended view of the hydrogen bond patterns of R-RR structure, highlighting the orientation of the interactions. a) Orthogonal BINOL-DACH chains, with arrows indicating their orientation, b) BINOL-DACH chains disposed in space to compare their hydrogen bonding directions.

Upon heating, the *R-RR* cocrystal shows a single endothermic melting event at 157°C (Figure SI-24). TGA analysis (Figure SI-13) shows degradation to occur upon melting.

The *R-RR* structure is readily obtained both from aprotic polar (EtOAc and ACN) or protic polar solvents (MeOH and EtOH) (Figure SI-1). However, from toluene and benzene, isostructural *R-RR*-solvent (1:1:1) cocrystal-solvates are obtained, driven by CH-π interactions (Figures 3 and SI-1). Although benzene has higher symmetry than toluene, isostructural solid forms can be obtained, explained by the disorder of toluene in the crystal lattice.

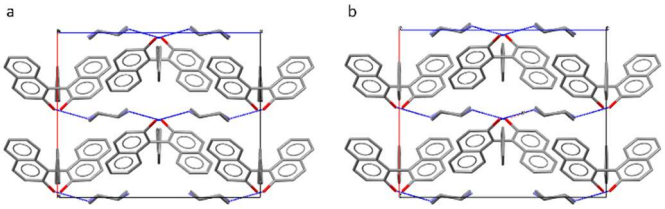

Figure 3. Crystal packing of the *R-RR* cocrystal solvates, view along b-axis, a) *R-RR*-tolu, b) *R-RR*-benz.

Compared to the non-solvated forms, the main hydrogen bonding motifs between alternating BINOL and DACH molecules are preserved (Figure 4, Tables SI-3 and SI-5). However, additional CH-π interactions are established between the aromatic solvent molecules and the naphthyl units of BINOL (Tables SI-4 and SI-6 and Figures SI-9 and SI-10) and all hydrogen bonding chains oriented parallel to one another.

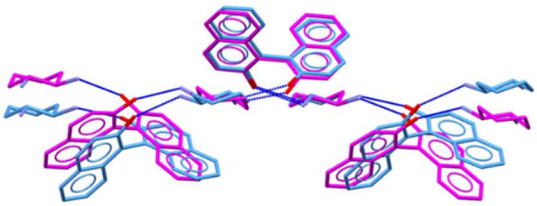

Figure 4. Superposition of *R-RR* (pink) and *R-RR*-tolu (blue) chains.

Thermal analyses confirm the loss of 1 equivalent of solvent upon heating, resulting in broad desolvation endotherms in the DSC analyses (Figures SI-25 and SI-26) starting around 90°C, and a clear desolvation step-weight loss in the TGA analyses (Figures SI-14 and SI-15). After desolvation, both structures lead to the obtention of the stable *R-RR* cocrystal phase (Figure SI-2).

Combination 2: (S)-BINOL and (R,R)-DACH

When combining (*S*)-BINOL and (*R,R*)-DACH, slurry experiments in all tested solvents allowed to obtain the already reported *S-RR* cocrystal (CDCC ref code: SUVNEC[16]) (Figure SI-3).

The *S-RR* phase contains two formula units per asymmetric unit, with (*S*)-BINOL and (*R,R*)-DACH engaged in similar hydrogen bonding interactions as observed for the *R-RR* cocrystals (Figure 5, Table SI-7).

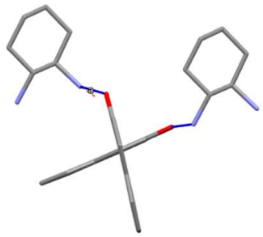

Figure 5. Extended view of the hydrogen bonding patterns for both BINOL molecules of the S-RR structure, highlighting the orientation of the interactions.

Thermal analysis shows a single endothermic melting event at 137°C (Figure SI-27), followed by degradation. TGA analysis (Figure SI-16) shows degradation to occur upon melting. The 20°C lower melting point of the *S-RR* diastereomer compared to the *R-RR* one, indicates this diastereomer to be the less stable one.

Interestingly, *S-RR*-toluene or -benzene solvates are not found. In a previous study, we have reported a similar solvent effect, allowing only one specific chiral combination to be solvated.[15]

Combination 3: (rac)-BINOL and (R,R)-DACH

When racemic BINOL is combined with enantiopure DACH, effective resolution occurs in acetonitrile, as well as in toluene and benzene (Figures SI-46 to SI-48). In the former solvent, the *R-RR* cocrystal is obtained – this result confirms the *R-RR* diastereomer to be more stable (less soluble) compared to the *S-RR* combination. For the latter two solvents the *R-RR*-solvent cocrystal-solvate comes out (Figure SI-4), keeping in mind the *S-RR*-solvates likely do not exist. (*S*)-Binol remains dissolved in the mother liquor and does not crystallize under the conditions studied. Acetonitrile, toluene, and benzene can therefore effectively be used to resolve BINOL using enantiopure DACH as the resolution agent.

We can, here, already highlight the importance of the solvent on the resolution potential, as resolution is no longer possible when using EtOAc, MeOH or EtOH. For all of these, a multicomponent solvate phase is formed, which combines (*rac*)-BINOL and (*R,R*)-DACH (Figure SI-4). This result shows how strongly a resolution potential can depend on the solvent nature.

The use of EtOAc resulted in the formation of a crystalline material, which we were unsuccessful in characterizing structurally. To obtain information on the composition of the obtained phase, the powder was analyzed by NMR, TGA, DSC, and *c*HPLC. ^{1}H NMR analysis shows the obtention of a phase composed of 1 equivalent of BINOL, 1 equivalent of DACH and 0.5 equivalent of EtOAc (Figure SI-49). Upon heating (Figures SI-19, SI-30), this compound shows a clear desolvation signal to occur at around 70-80°C, corresponding to 0.6 equivalent of EtOAc, confirming the presence of solvent in the structure. *c*HPLC analysis shows the obtention of a racemic mixture of BINOL (Figure SI-44), allowing us to establish formation of a multicomponent 2*rac*-2*RR*-EtOAc (2:2:1) phase.

The solid phase obtained in methanol shows a XRPD pattern superposable to the simulated *rac-rac*-MeOH (1:1:1) pattern (Figure SI-4), which will be discussed for Combination 5 ((*rac*)-BINOL and (*rac*)-DACH). We therefore suspect the *rac-rac*-MeOH phase to form a solid solution with respect to DACH. Upon heating (Figures SI-17, SI-28), the *rac-RR*-MeOH solid phase remains stable up to 60-65°C. Thermal analyses confirm the loss of 1 equivalent of MeOH upon heating, with a clear solvent step-weight loss (Figures SI-17), and large desolvation endotherm (Figures SI-28) starting around 70°C.

The solid phase obtained in ethanol shows a unit cell composed of four negatively charged molecules of BINOL (2 *R* and 2 *S*), and four positively charged molecules of (*R,R)*-DACH, three EtOH molecules, and one water molecule (Figure 6). Within the lattice, disorder between EtOH and water molecules occurs (Figure SI-11, Table SI-8). Upon heating (Figure SI-29), the 4*rac*-4*RR*-3EtOH-H_2O (4:4:3:1) compound remains stable up to 75°C, at which point a large endothermic event occurs, corresponding to a combined desolvation and melting event. TGA analysis confirms a two-step weight loss corresponding to the desolvation of 3 equivalents of EtOH and 1 equivalent of H_2O (Figure SI-18).

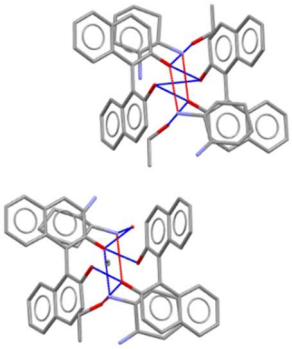

Figure 6. Asymmetric unit of 4*rac*-4*RR*-3EtOH-H_2O, view along *a*-axis.
EtOH and H_2O molecules are disordered. Here, only one possibility is shown for clarity.

Desolvation of the powders recovered from slurrying (*rac*)-BINOL and (*R,R*)-DACH in EtOAc and MeOH (or EtOH) led to the obtention of two different diffraction patterns, likely corresponding to different polymorphs of the *rac-RR* combination (Figure SI-5). These *rac-RR* solid forms cannot be accessed directly, but require passage through a solvated phase, again highlighting the crucial role a solvent can play.

Combination 4: (R)-BINOL and (rac)-DACH

When components (*R*)-BINOL and (*rac*)-DACH are slurried in EtOAc, ACN, MeOH, or EtOH, the resulting powders exhibit XRPD patterns identical to that of the *R-RR* cocrystal. In contrast, when slurried in toluene or benzene, two cocrystal-solvates are obtained, respectively *R-RR*-tolu and *R-RR*-benz (Figure SI-6).

Each phase was analyzed by DSC (Figures SI-37 to SI-42). This showed that a mixture of both diastereomers *R-RR* and *R-SS* was obtained when EtOAc was used as solvent (Figure SI-39), the amount of *R-SS* being too small to be visible by XRPD. On the other hand, the possibility of chiral resolution of (*rac*)-DACH with (*R*)-BINOL as the resolving agent is demonstrated in the five other solvents: toluene, benzene, ACN, MeOH, and EtOH. While *R-RR*-solvent (in toluene and benzene) or *R-RR* (in ACN, MeOH, and EtOH) crystalline forms are

obtained, (*S,S*)-DACH remains dissolved in the mother liquor and does not crystallize under the conditions studied.
Moreover, this, once more, highlights the increased stability of the *R-RR* diastereomer with respect to the *R-SS* (equivalent to the *S-RR*) cocrystal phase.

Combination 5: (rac)-BINOL and (rac)-DACH

The role of the solvent is even more crucial when combining both racemates.
Using toluene and benzene as the solvent yields XRPD patterns superimposable with those of the simulated pattern of the cocrystal-solvate *R-RR*-solvent (Figures 7a and 8a), seemingly indicative of a conglomerate formation. Such a behavior would allow simultaneous resolution by preferential crystallization of both compounds.[11–14] Indeed, in the literature, the *R-RR*-tolu cocrystal-solvate was referenced as a conglomerate.[16] To gather further evidence confirming this hypothesis and disprove the occurrence of a solid solution, *c*HPLC of hand-picked crystals obtained by a slow-evaporative experiment of (*rac*)-BINOL and (*rac*)-DACH in toluene was carried out. The analysis showed both enantiomers (*R*)- and (*S*)-BINOL coexisting in the same crystal (Figure 7b). Therefore, we have identified these crystals not as true conglomerates but as being twinned, containing domains of both *R-RR* and *S-SS*.

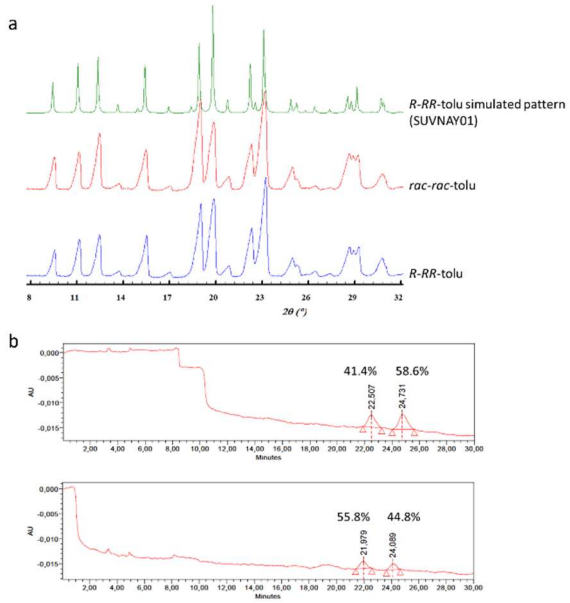

Figure 7. a) Comparison of the XRPD simulated pattern of *R-RR*-tolu cocrystal-solvate (green) with XRPD patterns of the solids obtained by slurrying in toluene (*R*)-BINOL and (*R,R*)-DACH (blue) and (*rac*)-BINOL and (*rac*)-DACH (red). b) *c*HPLC chromatograms of randomly chosen single crystals showing a racemic composition in BINOL.

A similar behavior was observed for the benzene solvate, with both XRPD patterns of enantiopure and racemic cocrystals superimposable (Figure 8a), but with *c*HPLC of a single crystal showing both enantiomers (Figure 8b), again suggesting the occurrence of twining.

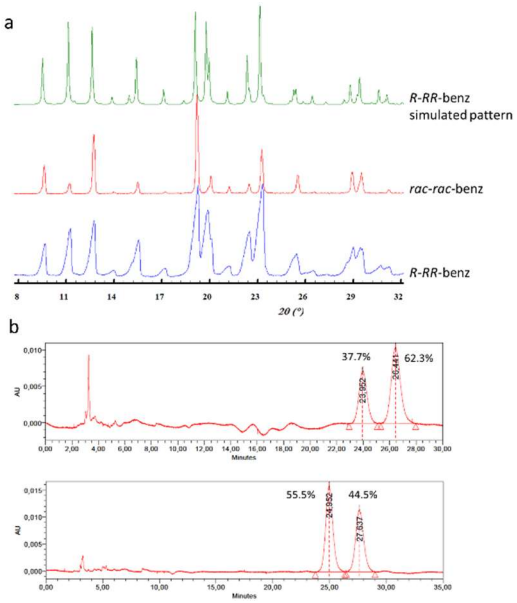

Figure 8. a) Comparison of the XRPD simulated pattern of R-RR-benz cocrystal-solvate with XRPD patterns of the solids obtained by slurrying in benzene (R)-BINOL and (R,R)-DACH (blue) and (rac)-BINOL and (rac)-DACH (red). b) cHPLC chromatograms of randomly chosen single crystals showing a racemic composition in BINOL.

Using any other selected solvent, both racemic compounds combine in a single solid form (Figure SI-7). Therefore, none of the other investigated solvents allowed the formation of conglomerates, rendering simultaneous chiral resolution of BINOL or DACH by preferential crystallization impossible.

ACN led to a *rac-rac* (1:1) cocrystal (Figure 9, Table SI-11) with a (1:1) stoichiometric ratio. Upon heating, the *rac-rac* cocrystal shows a single endothermic melting event at 146°C (Figure SI-34). TGA analysis (Figure SI-21) shows degradation to occur upon melting

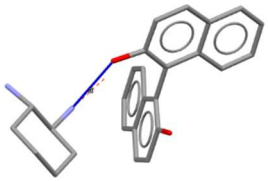

Figure 9. Asymmetric unit of the *rac-rac* cocrystal, view along *c*-axis.

In EtOAc, two different structures are recovered. Indeed, the XRPD patterns of the slurry outcome and that simulated from the single crystal obtained by slow evaporation differ (Figure SI-7).
SC-XRD analysis of the phase obtained by slow evaporation shows the obtention of a *rac-rac*-EtOAc (1:1:1) cocrystal-solvate (Figure 10). EtOAc molecules are found disordered on an inversion, indicating the solvent molecules merely occupy cavities in the packing, rather than being strongly engaged in stabilizing the structure. This is also explained by the absence of hydrogen bonds with the EtOAc solvent molecule (Table SI-10).

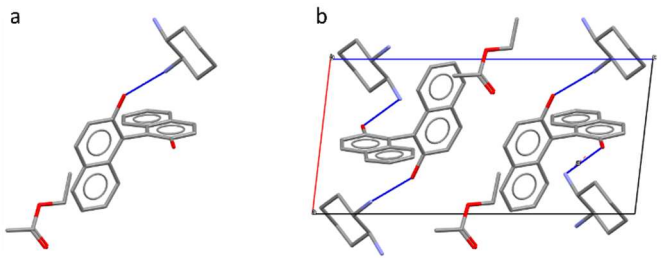

Figure 10. Structure of the *rac-rac*-EtOAc cocrystal-solvate obtained by slow evaporation, with the major compounds represented. a) Asymmetric unit, view along *b*-axis, b) Crystal packing, view along *b*-axis.
EtOAc molecules are disordered. Only one molecule is shown for clarity.

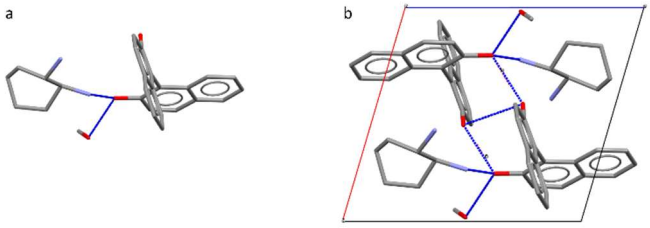

Figure 11. Structure of the *rac-rac*-MeOH cocrystal-salt-solvate, with the major compounds represented. a) Asymmetric unit, view along *b*-axis, b) Crystal packing, view along *b*-axis.
DACH molecules show *R-S* disorder. Only the most occupied molecule (51%) is shown for clarity.

To obtain information on the composition of the phase obtained from the slurry experiment in EtOAc, the filtrated powder was analyzed by NMR, TGA, DSC and *c*HPLC. ^{1}H NMR analysis shows the obtention of a phase composed of 1 equivalent of BINOL and 1 equivalent of DACH, without any EtOAc molecule (Figure SI-50). TGA analysis revealed a two-stage mass loss (Figure SI-20). The first mass loss occurs at 111°C and the material is completely degraded at 315°C. DSC analysis displayed a single melting peak with an onset at 145°C, consistent with a non-solvated phase (Figure SI-33). Finally, *c*HPLC analysis confirmed BINOL to be racemic (Figure SI-43). As the DACH molecule contains no chromatophores, we were unable, at first, to determine whether the compound is racemic or enantiopure. Therefore, these analyses collectively confirmed the formation of a new crystalline phase, which is likely either *rac-rac* (1:1) or *rac-RR* (1:1).

Both racemic BINOL and DACH are combined when using methanol as a solvent. SC-XRD analysis resulting from a slow evaporative experiment of (*rac*)-BINOL and (*rac*)-DACH in MeOH leads to the formation of the *rac-rac*-MeOH (1:1:1) cocrystal-salt-solvate, with a negatively charged BINOL molecule and positively charged DACH molecule (Figure 11, Table SI-9).
The simulated XRPD pattern matches that of the powder recovered from the (*rac*)-BINOL-(*R,R*)-DACH slurry experiment in MeOH (Figure SI-4). However, the structure formed is not a conglomerate as the material crystallizes in the centrosymmetric space group *P*-1. Therefore, both enantiomers of BINOL and DACH are present in the same crystal lattice (Figure 11b). Moreover, the component crystallized as a solid solution with respect to DACH. Indeed, while BINOL molecules are well ordered, DACH molecules exhibit *S/R* disorder with a ratio of 51/49 (Figure SI-12), explaining the good correspondence of XRPD patterns between *rac-rac*-MeOH and *rac-RR*-MeOH. TGA analysis shows desolvation of MeOH (Figure SI-22) occurring at 60°C. DSC analysis (Figure SI-35) shows a large endothermic event to occur upon heating, corresponding to desolvation of MeOH with an onset at 71°C, followed by an exothermic event, possibly being recrystallization, at 97°C. The resulting compound undergoes a small endothermic event at 100°C and finally, melts at 143°C.

In parallel, the slurry outcome of the mixture (*rac*)-BINOL and (*rac*)-DACH in EtOH could not be structurally characterized. ^{1}H NMR analysis was used to determine the composition of the phase, revealing it to consist of one equivalent of BINOL, one equivalent of DACH, and one equivalent of EtOH (Figure SI-45). This result is confirmed by TGA analysis (Figure SI-23). Indeed, the compound shows three distinct mass losses. The first one occurs at 60°C and is a desolvation step, corresponding in the loss of one molecule of EtOH. DSC analysis (Figure SI-36) confirms this desolvation event with an endothermic peak at 71°C, followed by melting of the resulting compound at 144°C. Finally, *c*HPLC analysis confirmed BINOL to be racemic (Figure SI-51), and as the DACH molecule contains no chromatophores, we were unable, at first, to determine whether the compound is racemic or enantiopure. These analyses allowed us to confirm the formation of a multicomponent phase which is either the *rac-rac*-EtOH (1:1:1) or *rac-RR*-EtOH (1-1-1) phase.

After their desolvation, powders recovered from slurrying *(rac)*-BINOL and *(rac)*-DACH in toluene, benzene, MeOH and EtOH exhibited identical XRPD patterns, which can be superposed to the one obtained from the slurry of (*rac*)-BINOL and (*rac*)-DACH in EtOAc (Figure SI-8). DSC analysis also showed a similar phase (Figures SI-31, SI-32, SI-35, and SI-36). These results allowed us to confirm the formation of the *rac-rac* (1:1) phase in EtOAc and the formation of the *rac-rac*-EtOH (1:1:1) phase in EtOH. It is interesting to observe that a different polymorph of this *rac-rac* cocrystal phase is obtained in ACN (Figure SI-8).

Conclusion

The main goal of this study was the rational and systematic analysis of the interactions when combining DACH and BINOL molecules in various stereochemical combinations in the presence of six solvents with varying polarity and proticity. This investigation resulted in the identification of 11 multicomponent crystalline phases, including eight previously unreported forms. Among these, five were structurally resolved in this study (*R-RR*-benz, *rac-rac*, *rac-rac*-EtOAc, *rac-rac*-MeOH, and 4*rac*-4*RR*-3EtOH-1H_2O).

By these results we reveal how solvent properties influence the crystallization outcome.

The two non-polar and aprotic solvents, toluene and benzene, which are both aromatic, yielded similar results, due to their CH-π interactions with BINOL. Here, their aromatic nature significantly influences crystallization outcomes.
Polar aprotic solvents, ethyl acetate and acetonitrile, show divergent behavior. Their structural differences significantly affect the crystallization outcome.
Finally, polar protic solvents, methanol and ethanol, both small alcohols, yielded similar results.

Our results provide strong evidence that the ability to achieve diastereomeric resolution is highly solvent-dependent. Although BINOL and DACH can, in principle, be resolved by diastereomeric crystallization, only three solvents (toluene, benzene, acetonitrile) allow resolving both BINOL by DACH and vice versa. This underscores that for successful resolution processes not only the right combination of target and resolution agent is crucial but also the choice of solvent.

Notes and references

1 H. Lorenz and A. Seidel-Morgenstern, *Angew. Chem. Int. Ed.*, 2014, **53**, 1218–1250.
2 J. I. Putman and D. W. Armstrong, *Chirality*, 2022, **34**, 1338–1354.
3 R. Kaviani, A. Jouyban and A. Shayanfar, *CrystEngComm*, 2023, **25**, 6120–6131.
4 Y. Teng, C. Gu, Z. Chen, H. Jiang, Y. Xiong, D. Liu and D. Xiao, *Chirality*, 2022, **34**, 1094–1119.
5 J. Sui, N. Wang, J. Wang, X. Huang, T. Wang, L. Zhou and H. Hao, *Chem. Sci.*, 2023, **14**, 11955–12003.
6 F. Zhou, C. Body, K. Robeyns, T. Leyssens and O. Shemchuk, *CrystEngComm*, 2023, **25**, 3060–3065.
7 G. Springuel and T. Leyssens, *Cryst. Growth Des.*, 2012, **12**, 3374–3378.
8 T. Nulek, R. Klaysri, R. Cedeno, P. Nalaoh, S. Bureekaew, V. Promarak and A. E. Flood, *ACS Omega*, 2022, **7**, 19465–19473.
9 O. Sánchez-Guadarrama, F. Mendoza-Navarro, A. Cedillo-Cruz, H. Jung-Cook, J. I. Arenas-García, A. Delgado-Díaz, D. Herrera-Ruiz, H. Morales-Rojas and H. Höpfl, *Cryst. Growth Des.*, 2016, **16**, 307–314.
10 S. Songsermsawad, P. Nalaoh, V. Promarak and A. E. Flood, *Cryst. Growth Des.*, 2022, **22**, 2441–2451.
11 X. Buol, C. Caro Garrido, K. Robeyns, N. Tumanov, L. Collard, J. Wouters and T. Leyssens, *Cryst. Growth Des.*, 2020, **20**, 7979–7988.
12 F. Zhou, O. Shemchuk, M. D. Charpentier, C. Matheys, L. Collard, J. H. ter Horst and T. Leyssens, *Angew. Chem. Int. Ed.*, 2021, **60**, 20426–20430.
13 L. Wang, N. Wang, J. Sui, S. Sun, Z. Feng, G. Li, H. Hao and L. Zhou, *Cryst. Growth Des.*, 2023, **23**, 5641–5650.
14 P. Rapeenun, C. J. J. Gerard, C. Pinètre, Y. Cartigny, P. Tinnemans, R. De Gelder, A. E. Flood and J. H. Ter Horst, *Cryst. Growth Des.*, 2024, **24**, 480–490.
15 J. de Meester, O. Shemchul, L. Collard, W. Johan, S. Baillieux, K. Robeyns and T. Leyssens, *CrystEngComm*, 2024, **26**, 2056–2059.
16 M. Ratajczak-Sitarz, A. Katrusiak, K. Gawrońska and J. Gawroński, *Tetrahedron: Asymmetry*, 2007, **18**, 765–773.
17 CrysAlisPro, Version 1.171.37.35; Rigaku Oxford Diffraction.
18 G. M. Sheldrick, *Acta Crystallogr., Sect. A: Found. Adv*, 2015, **71**, 3–8.
19 G. M. Sheldrick, *Acta Crystallogr., Sect. C: Struct. Chem.*, 2015, **71**, 3–8.
20 A. L. Spek, *Acta Crystallogr., Sect. D: Biol. Crystallogr.*, 2009, **65**, 148–155.
21 C. F. Macrae, I. Sovago, S. J. Cottrell, P. T. A. Galek, P. McCabe, E. Pidcock, M. Platings, G. P. Shields, J. S. Stevens, M. Towler and P. A. Wood, *J Appl Cryst*, 2020, **53**, 226–235.
22 M. Kawashima and R. Hirata, *BCSJ*, 1993, **66**, 2002–2005.
23 C. R. Bertsch, W. C. Fernelius and B. P. Block, *J. Phys. Chem.*, 1958, **62**, 444–450.
24 X. Ni, X. Li, Z. Li and J.-P. Cheng, *Org. Chem. Front.*, 2016, **3**, 1154–1158.